J Mater Sci (2022) 57:5346–5357

Polymers & biopolymers

Tuning thermal conductivity of surface-initiated polymer brushes

Wenhao Sha[1], Huizhong Wang[2], and Fenglin Guo[1,*]

[1] School of Naval Architecture, Ocean and Civil Engineering (State Key Laboratory of Ocean Engineering), Shanghai Jiao Tong University, Shanghai 200240, China

[2] School of Materials Science and Engineering, University of New South Wales, Sydney, NSW 2052, Australia

Received: 13 October 2021
Accepted: 20 January 2022
Published online: 11 February 2022

ABSTRACT

Surface-initiated polymer brushes are widely used in industrial applications owing to their programmable interfacial properties and manipulation over the harmonious combination of materials at the molecular level, particularly in surface-coating technologies. So far, surface-initiated polymer brushes are emerging as robust candidates for heat dissipation coatings. However, the brushes of carbon nanotubes, nanowires, or polymers show a terrible reduction of thermal conductivity, although a single carbon nanotube can exhibit a high value of thermal conductivity. Thus, how to control the thermal conductivity of surface-initiated polymer brushes remains a challenge for producing heat dissipation materials. Here we demonstrate programmable control of thermal conductivity of polymer brushes by tuning the grafted density on the target surface and the persistence length of polymer chains, using coarse-grained molecular dynamics (CGMD) simulations based on experimental data. Our simulation results show that the thermal conductivity of surface-initiated polymer brushes is anisotropic and a delicate balance between the grafted density and persistence length. Moreover, detailed structure analysis and phonon analysis are conducted to unveil the thermal characteristics of polymer brushes. We expect that our results may help broaden the industrial applications of surface-initiated polymer brushes.

Introduction

Reasonable regulation of heat energy is one of the crucial elements that enable our societies to develop and advance in a sustainable way, e.g., professional heat management helps alleviate the impact of temperature on the performance of equipment [1, 2]. Over the years, noteworthy efforts have been made in developing cutting-edge technologies to solve these issues [3, 4]. Among these techniques, nanotechnologies are one of the effective and promising

Handling Editor: Maude Jimenez.

Address correspondence to E-mail: flguo@sjtu.edu.cn

https://doi.org/10.1007/s10853-022-06945-y

technical roadmaps to tune thermal properties because they often exhibit surprising behavior [5]. With the continuous advancement of nanotechnology, it is found that the reasonable design of the microstructure of polymers can significantly improve the thermal conductivity of polymers [6]. Choy et al. [7] have testified that the in-plane thermal conductivity of ultrahigh molecular weight polyethylene could exceed 40 W/mK by increasing the crystallinity and rationally aligning the polymer chains. Even the thermal conductivities of commercially available microfibers are measured to be as high as 23 W/mK with optimized microstructure [8]. In comparison, general commercial polyethylene (PE) products are commonly regarded as thermal insulators with a thermal conductivity value of about 0.4 W/mK [9, 10].

During the last decade, one-dimensional or quasi-one-dimensional materials have attracted the attention of many researchers because of their excellent physical properties. For a single carbon nanotube (CNT), the thermal conductivity along the backbone $\kappa_{\parallel}$ of CNT exceed 10^3 W/mK [2]. However, the arbitrary-designed and unordered CNT-based forests, bundles, sheets, and networks show a terrible reduction of thermal conductivity, for example, $\kappa_{\parallel}$ of CNT forests [11] is reduced to 0.5–1.2 W/mK, $\kappa_{\parallel}$ is around 100 W/mK for CNT bundles [12], $\kappa_{\parallel}$ is about 43 W/mK for CNT sheets [13]. This sharp decrease in thermal conductivity is not a specific phenomenon for CNT and can also be found in silicon nanowire (NW) arrays [14], PE fibers [8], crystalline assemblies of PE [15], and poly-3,4-ethylene dioxythiophene (PEDOT) [16]. At present, people have realized the impact of the unreasonable design of microstructures on physical properties; besides, rational design of microstructures of existing materials has overwhelming advantages over synthesis of new materials because the former is more environmental-friendly and resource-saving.

Nowadays, interfacial nanotechnologies with surface-initiated polymer brushes have seen rising interest both in industry and academia due to their potential to improve interfacial performance [17]. The so-called surface-initiated polymer brushes usually consist of one-dimensional or quasi-one-dimensional materials, which are robust functional coating materials with unique end-anchoring structures and extraordinary physical characteristics. Most of these functionalities are achieved by chemically grafting one end of prefabricated one-dimensional or quasi-one-dimensional materials, especially polymer chains, at a specific density to a substrate. Specifically, the synthesis method [17] of surface-initiated polymer brushes can be roughly divided into two types: "grafting to" and "grafting from", which are consistent with their synthetic approach. In the former approach, the polymer chains with functional groups that can react or interact with the target substrate are first prepared, and then the prefabricated polymers are tethered to the substrate through chemical reaction subsequently. In contrast, in the "grafting from" method, the polymer brushes gradually grow from the tethered initiators on the substrate. The different types of polymer chains tethered on the target surface will provide the substate with desirable properties [18] including controllable wettability, corrosion resistance, adhesive performance, lubrication and friction properties. Besides, as the rational structural design of materials has the potential to improve the efficiency of interfacial heat exchange, research interest in the optimal design of surface-initiated polymer brushes has grown rapidly in heat management. Cola et al. [19] have experimentally testified that the improvement of alignment in polymer brushes further enhances the thermal conductivity. Mukherji et al. [20] numerically prove that the thermal conductivity of polymer forests is an intriguing balance between the interaction of non-bonded polymer chains and the bending of polymer chains. However, the thermal transportation for surface-initiated polymer brushes consisting of a wide range of one-dimensional or quasi-dimensional materials is still not clear.

In this study, we report simulation results of thermal transportation in surface-initiated polymer brushes on a two-dimensional flat plane using a multiscale molecular dynamics method. We map the physical properties of polymer chains into a CGMD model by a simple strategy. Detailed equilibrium molecular dynamics simulations using the Green–Kubo method are employed to obtain the thermal conductivity of different surface-initiated polymer brushes. Furthermore, structure analysis and phonon density of states (PDOS) are used to illustrate the change of thermal conductivity in different polymer brushes. Our purpose is to use a generic model to unveil the thermal characteristics of an extensive range of materials with similar structural features.

Simulation details and methods

Simulation details

To mimic the configuration of real surface-initiated polymer brushes, we use a simple mapping scheme to transform the nanoscale physical features into a coarse-grained (CG) model. Because one-dimensional and quasi-one-dimensional materials are the main components of polymer brushes, surface-initiated polymer brushes inherit their excellent flexibility. For these materials, their intrinsic flexibility is governed by persistence length l_p. The polymer chain with a high value of l_p usually possesses high bending stiffness, which is easier to keep the shape of a linear rod. Notably, the polymer chain with a considerably small value of l_p is soft and easy to collapse into a pile. To model this feature into our coarse-grained model, we summarize the relationship between persistence length and diameter of several one-dimensional and quasi-one-dimensional materials in Fig. 1. This perspective provides essential information about the length scale of a single polymer chain in our CG models.

In our CG model, we consider a spherical bead represents several monomers, and the diameter of the bead is set as σ. Thus, the range of persistence length is circumscribed from 0.65σ to $5 \times 10^5\sigma$. As the persistence length ($l_p = \frac{k}{k_B T}$) is positively dependent on the bending stiffness, it is convenient to change the persistence length by changing the bending stiffness (k). The bending energy of a polymer chain is defined as: $E_B = \frac{k}{2}\int_0^L \left(\frac{\partial T}{\partial s}\right)^2 ds$ [30], where L is the length when the polymer chain is straightened and not extensible, $\mathbf{T}$ is the position vector of a CG bead, k is the bending stiffness reflecting the flexibility of a polymer chain, and $\frac{\partial T}{\partial s}$ represents the degree of local bending. As the bending energy of this model is given as:

$$E_B = \frac{k}{2}\int_0^L \left(\frac{\partial T}{\partial s}\right)^2 ds \tag{1}$$

the discretized version of Eq. (1) can be illustrated as follows:

$$\begin{aligned} &\approx \frac{k}{2r_0}\sum_i \left(T_{i+1}^2 + T_i^2 - 2\cos\alpha\right) \\ &= \frac{k}{r_0}\sum_i (1-\cos\alpha) \\ &= \frac{k}{r_0}\sum_i (1-\cos(\pi-\theta)) \\ &= \frac{l_p k_B T}{r_0}\sum_i (1-\cos(\pi-\theta)) \end{aligned} \tag{2}$$

where θ is the bond angle between the bond vectors (among three successive CG beads), α is the complementary angle, and r_0 is the balanced bond length.

The Kremer–Grest model [31] is employed to describe the CG polymer chain in this work, which has been testified to be able to describe the thermal transportation of polymers [6, 20]. Within our CG model, consecutively bonded spherical beads with the mass of m form a polymer chain. The nonbonded interactions, which are mainly the van der Waals (vdW) interactions, within and between polymer chains are expressed by a Lennard–Jones (LJ) potential:

$$U_{LJ}(r_{ij}) = 4\varepsilon\left[\left(\frac{\sigma}{r_{ij}}\right)^{12} - \left(\frac{\sigma}{r_{ij}}\right)^{6}\right], r_{ij} < r_c \tag{3}$$

All other physical parameters are deduced and based on these three fundamental reduced Lennard–Jones units (ε, σ, and m are the reduced units of energy, length, and mass, respectively.) with Boltzmann constant set as $k_B = 1$.The time unit can then be deduced to $\tau = \sigma(m/\varepsilon)^{1/2}$. The cutoff radius is set as $r_c = 1.12246\sigma$ in all types of interactions for enhancing the calculation efficiency. Within the Lennard–Jones potential, σ is the point where the LJ potential crosses the zero energy line, and the parameter ε equals the strength of interaction.

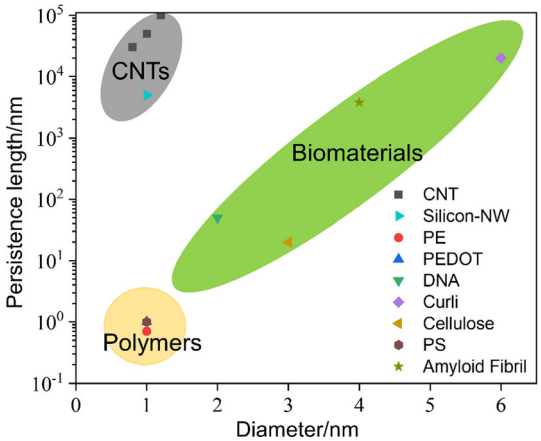

Figure 1 Persistence length versus diameter of different single chains [21–29].

For bonded beads, the Kremer-Grest model uses finite extensible nonlinear elastic (FENE) bonds to connect each bead. The FENE bond potential can be expressed as:

$$U_{\text{bond}}(r_{ij}) = -0.5k_{\text{fene}}R_0^2 \ln\left[1 - \left(\frac{r_{ij}}{R_0}\right)\right] \quad (4)$$

which can effectively confine the maximum of bond length to $R_0 = 1.5\sigma$. The bond strength is set to $k_{\text{fene}} = 30.0\varepsilon \cdot \sigma^{-2}$, and the balanced bond length is $r_{\text{balance}} = 0.97\sigma$. The following equation defines the total energy of a polymer brush system:

$$U_{\text{total}} = U_{\text{bond}} + U_{\text{LJ}} + U_{\text{angle}} + U_{\text{kinetic}} \quad (5)$$

Each polymer chain in all brush systems consists of 501 beads. The contour length of a polymer chain is $N_l \cong 500\sigma$, because the balanced bond length is $r_{\text{balance}} = 0.97\sigma$. Furthermore, the first beads are randomly fixed onto a square plane with lateral dimensions $L_x = L_y \cong 35\sigma$, and the chains are placed perpendicular to the square plane along the z direction in the initial configuration. The surface grafted density ρ_{grafted} is varied from $0.2\ m \cdot \sigma^{-2}$ to $0.65\ m \cdot \sigma^{-2}$. ρ_{grafted} is obtained by dividing the number of fixed CG beads on the surface by the total surface area ($L_x L_y$). Periodic boundary conditions are applied in the x and y directions, and fixed boundary condition is applied in the z direction.

Simulations are performed in two steps: the initial relaxation of polymer brushes, and the calculation of physical properties including thermal conductivity, density, virial stress, and phonon analysis. The initial relaxation is carried out under the canonical ensemble (NVT ensemble) with a timestep of $\Delta t = 0.001\tau$, and the relaxation is run for $10^6\tau$. The NVT ensemble is realized by coupling the Langevin thermostat and microcanonical ensemble (NVE ensemble). The Langevin thermostat possesses a damping constant $\gamma = 1\tau^{-1}$ and $T = 1\varepsilon k_{\text{B}}^{-1}$ in the initial equilibration, and the NVE ensemble is used for updating the position and velocity of CG beads. It should be emphasized that only thermal conductivities are calculated in the NVE ensemble, and the Langevin thermostat is decoupled in this process. The equations of motion are integrated using the velocity Verlet algorithm, and all the simulations are performed using the LAMMPS package [32].

Besides, one should notice that a simple CGMD model with artificially selected features is not suitable for elucidating all the physical properties of polymer brushes. Our purpose is trying to explore the effect of the morphological characteristics of surface-initiated polymer brushes on thermal transportation through numerical calculations. Also, we try to give rudimentary explanations of the reduction of thermal conductivity observed in experiments [13, 33] using a simple CGMD model.

Calculation of thermal conductivity and virial stress

After the preparation and equilibrium of initial configurations, the components of κ are calculated using the Green–Kubo method in the microcanonical ensemble (NVE ensemble). The equations of motion are integrated in the NVE ensemble with a timestep of $10^{-3}\tau$, and the estimation of the heat flux auto correlation ($\text{HACF}(t) = \langle J(t)J(0)\rangle$) is calculated by sampling the heat flux vector $J(t)$. Here, the correlation function is acquired in a time length of $2 \times 10^3\tau$ during a total simulation time of $2 \times 10^5\tau$; then, ten different simulation results will be obtained. Finally, κ is calculated by averaging these different plateau values of Green–Kubo integral for the component along the chain orientation direction, i.e., z direction,

$$\kappa_{\parallel} = \frac{V}{k_{\text{B}}T^2}\int_0^{\infty}\langle J_z(t)J_z(0)\rangle \mathrm{d}t \quad (6)$$

and in the lateral directions, i.e., x and y directions,

$$\kappa_{\perp} = \frac{V}{2k_{\text{B}}T^2}\int_0^{\infty}\left[\langle J_x(t)J_x(0)\rangle + \langle J_y(t)J_y(0)\rangle\right]\mathrm{d}t \quad (7)$$

It should be noted that every surface-initiated polymer brush has a certain number of fixed beads. However, these beads are not treated as rigid bodies. In order to make the simulations conformable to the Geen–Kubo method, several virtual springs are attached to the fixed beads. Therefore, the fixed beads can still oscillate at their initial position and keep the shape of surface-initiated polymer brushes.

Figure 2 is a numerical example for calculating $\kappa_{\parallel(0)}$ of a fully extended chain with two fixed ends with $l_{\text{p}} = 10$. It should be noted that Fan et al. prove the many-body heat flux is not correct in LAMMPS [34]. As we introduce the angle potential in this work, a many-body heat flux corrected LAMMPS version is used for the computation of thermal conductivity [35]. The virial stress $\sigma_{\parallel}$ is calculated using the

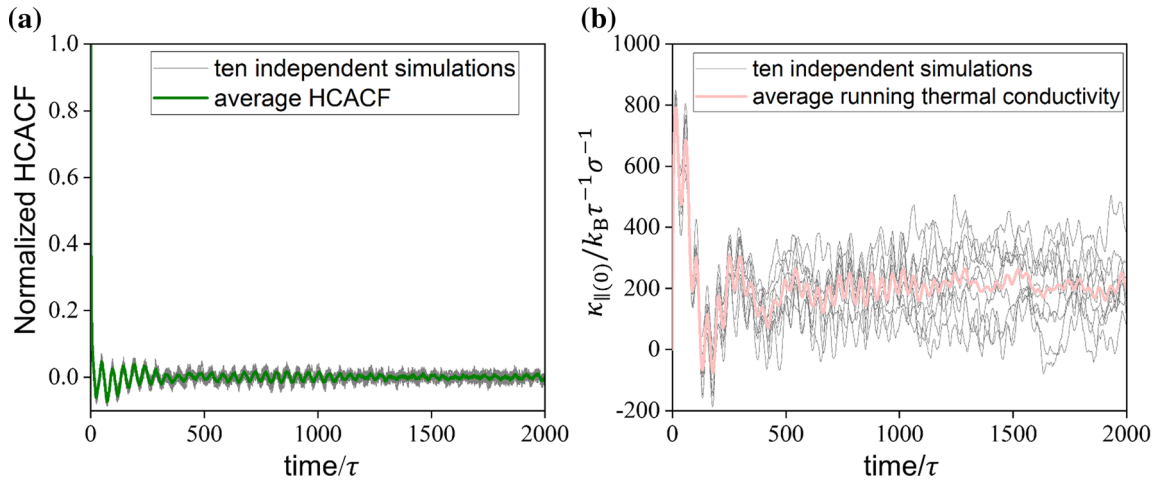

Figure 2 **a** Heat current autocorrelation function (HCACF) versus time, **b** $\kappa_{\|(0)}$ versus time.

standard subroutine in LAMMPS and following the procedure in the previous study [36].

Calculation of phonon density of states

The calculation of phonon density of states (PDOS) of materials is an effective way to describe phonon activities [4], which also provides explanations for the change of thermal conductivity. The PDOS is computed by integrating the fourier transform [37] of the velocity autocorrelation function (VACF) of a selected group of atoms as follows:

$$\mathrm{PDOS}(\omega) = \int_{-\infty}^{\infty} e^{i\omega t}\mathrm{VACF}(t)\mathrm{d}t \tag{8}$$

where $\mathrm{PDOS}(\omega)$ is the entire PDOS at the vibrational frequency ω and $\mathrm{VACF}(t)$ is described as:

$$\mathrm{VACF}(t) = \frac{1}{N}\sum_{i}^{N}\langle v_i(0)v_i(t)\rangle \tag{9}$$

$v_i(0)$ is the velocity vector for ith particle at time origin, $v_i(t)$ is the velocity vector for ith particle at time origin t, N is the number of the selected atoms. The ensemble average (denoted by $\langle\cdots\rangle$) in VACF is realized by time-average in molecular dynamics simulations over a period of 3τ, with the velocities extracted from the simulation under NVT ensemble every 0.001τ. For decomposed PDOS [38], the correlation function is calculated as $v_{ix}(0)v_{ix}(t) + v_{iy}(0)v_{iy}(t)$ and $v_{iz}(0)v_{iz}(t)$ for the directions vertical to the polymer chain and along the polymer chain, respectively. The peak of $\mathrm{PDOS}(\omega)$ predicates more states are occupied by the phonons with frequency ω. Note that when no phonon with the frequency of ω exists in polymer brushes, $\mathrm{PDOS}(\omega)$ is equal to 0.

Calculation of phonon participate rate

The calculation of phonon participation ratio (PPR) is another efficient technique providing perspectives into the phonon activities, especially for quantitatively describing the phonon mode localization, e.g., PPR equals 1 if all atoms participate in the heat conduction; otherwise, PPR equals to $1/N$ if only one atom participates in the heat conduction. That is, if the PPR increases, the localization of phonon modes will be mitigated. Therefore, the thermal conductivity will be higher. The PPR at any temperature can be calculated conveniently from the molecular dynamics simulations without the calculation of lattice dynamic [4], and is defined as [39, 40]:

$$\mathrm{PPR}(\omega) = \frac{1}{N}\frac{\left(\sum_i \mathrm{PDOS}_i(w)^2\right)^2}{\sum_i \mathrm{PDOS}_i(w)^4} \tag{10}$$

Results and discussions

Thermal conductivity of a single polymer chain

As mentioned in the introduction, a single polymer chain can exhibit a high thermal conductivity. Related numerical efforts have predicted that the thermal conductivity of a single polyethylene chain to be as high as 350 W/mK using all-atom molecular dynamics simulations [41]. To explore the influence

on the thermal conductivity of a single chain, we firstly consider only one chain in a crowded environment. Then we use a single chain with no interactions induced by other chains in a three-dimensional fixed boundary box for comparison. The grafted polymer brush to a two-dimensional rigid substrate is depicted in Fig. 3a, with the first bead of each polymer chain fixed to the substrate. All polymer brushes are configured in a rectangular box of dimensions $35\sigma \times 35\sigma \times 502\sigma$ (x, y, z, respectively). Periodic boundary conditions are applied in x and y directions, and fixed boundary conditions is used in z direction. Figure 3b is a configuration when a single polymer chain is fully extended in a three-dimensional fixed boundary condition. For the single chain with two fixed ends, the dimensions of the simulation box are $15\sigma \times 15\sigma \times 502\sigma$ (x, y, z, respectively) in order to save memory and reduce computation load in simulation.

The line chart of Fig. 4a depicts how the longitudinal thermal conductivity of a single polymer chain with two fixed ends $\kappa_{\parallel(0)}$ depends on the persistence length. We first focus on the red region of the line chart in Fig. 4a, where the longitudinal thermal conductivity is positively correlated with persistence length. However, the thermal conductivity decreases as the persistence length increases in the blue region, and then the thermal conductivity saturates in the green region. One should notice that for a polymer chain with unconstrained ends, its thermal conductivity is positively dependent on the persistence length. The decrease in the thermal conductivity in Fig. 4a is mainly due to the overall rotation of the chain relative to the axis of its initial position when l_p reaches a high value. In Fig. 4b, for the calculation of $\kappa_{\parallel(0)}$ in a brush, we randomly choose one chain in each polymer brush for computation of $\kappa_{\parallel(0)}$ in the crowded environment. It can be seen that, within the entire range of persistence length, $\kappa_{\parallel(0)}$ in a brush is reminiscently smaller than $\kappa_{\parallel(0)}$ of a single chain with two fixed ends. This sharp decrease of $\kappa_{\parallel}$ can also be seen in CNT forests and sheets [11, 13, 33]. Moreover, we find that with the increase in the grafted density, $\kappa_{\parallel(0)}$ in a brush is improved considerably. Furthermore, the collision between chains, the twinning of chains, and the rotation of chains are all inevitable in reality and simulations, which may be the reasons for the nonmonotonic increase of $\kappa_{\parallel(0)}$ when increasing the persistence length shown in Fig. 4b. We believe if these factors can be reduced or controlled, the thermal conductivity of a single chain in a crowded environment will be further improved.

A single polymer chain in a polymer brush configuration has two different modes of heat transfer: the heat transfer along the backbone of a chain is usually dominated by repeated covalent bonds; the heat transfer between chains is governed by the vdW interactions. Previous perspectives believe the longitudinal thermal conductivity of polymers is dominated by the bonded interaction because the strength of a covalent bond is about 100 times larger than that of vdW interactions. However, we find $\kappa_{\parallel(0)}$ of a single polymer chain in a brush is a delicate balance of its persistence length and the grafted density, and the persistence length and the grafted density are found to largely influence the morphology of a polymer system [30]. Therefore, we speculate that the maintenance of a rational and ordered micro-

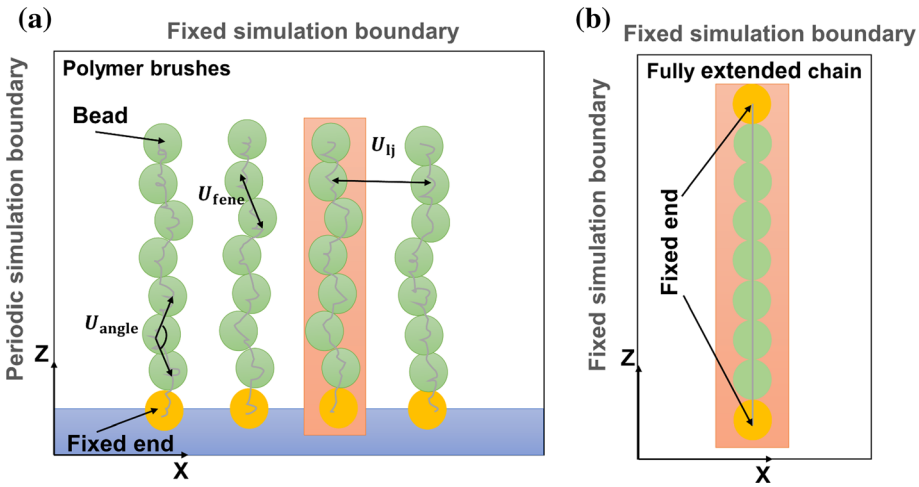

Figure 3 **a** Schematic diagram of surface-initiated polymer brushes represented by bead spring chains, along with the interactions involved in the brush and the boundary conditions of the simulation box. Yellow-colored beads are fixed to the rigid substrate. **b** A single polymer chain with two fixed ends (yellow-colored beads) to form a fully extended configuration in a simulation box.

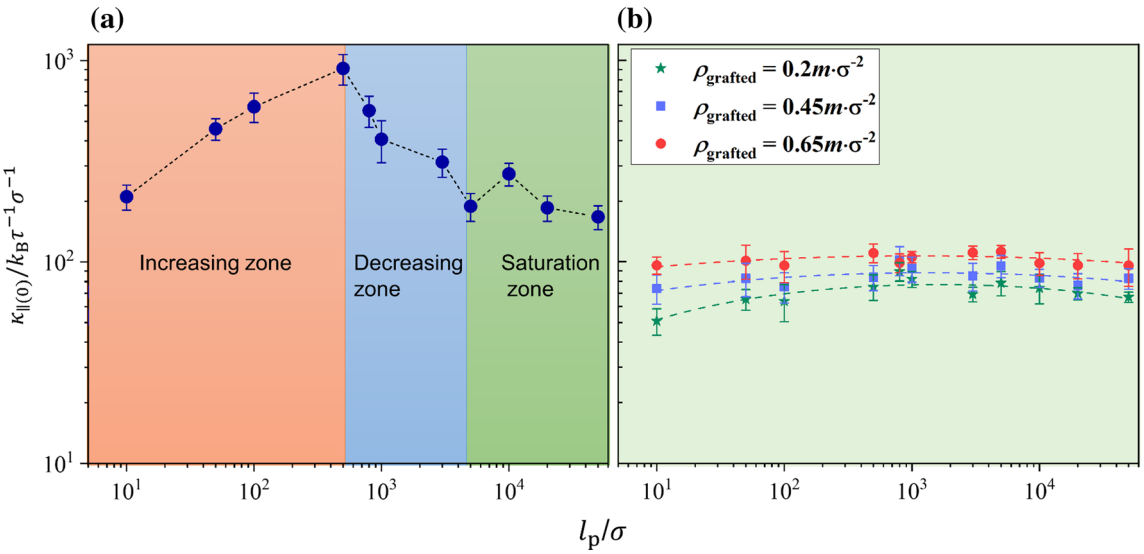

Figure 4 **a** Thermal conductivity of a fully extended polymer chain varying with the persistence length. Note that the distance between these two fixed ends is 501 $r_{balance}$, and the normalization volume in the Green–Kubo formula is taken as the volume of one chain, i.e., $v = 500\ v_{bead}$ with v_{bead} being the volume of one bead. **b** Thermal conductivity of a single polymer chain in a crowded environment with different grafted densities. The dashed line is a polynomial fit to the data.

morphology of a polymer chain has a crucial impact on improving thermal conductivity.

Density distribution, stress, and thermal conductivity

Then we start by calculating the number density distribution along the longitudinal direction for each polymer brush. It is expected that the orientation of every bond of a fully extended polymer chain should be aligned in one direction. Thus, the height of the polymer chain should be equal to the contour length (500 σ), and the beads should be distributed equally along the longitudinal backbone direction, i.e., the z direction. The green lines in Fig. 5a–c indicate the number density distribution along the z direction for polymer brushes when all the chains are fully extended. However, we find that polymer brushes with different grafted densities have a similar density concentration phenomenon. The density concentration indicates the disorder of bond orientation; therefore, the height of a polymer chain in a polymer brush is always smaller than its contour length. With the increase in the persistence length, the degree of density concentration will be alleviated. Furthermore, for polymer chains with a smaller persistence length, e.g., $l_p = 10\sigma$, it can be seen that $\rho_{\parallel}$ sketches show ridges at the top interface. The increment of the grafted density can effectively lower down the ridge.

The density concentration also gives a stress concentration, as shown in Fig. 5d–f. The stress concentration is caused by bending in chains and entangling between chains, which also means the aggregation of kinks [42]. Since the kinks can be considered as a phonon scattering center, reducing the number of kinks is beneficial for phonon propagation. In essence, the uniform distribution of polymer beads in three-dimensional space, i.e., no bending or curling for polymer chains will give a fairly high thermal conductivity, however, it is hard to achieve. Increasing the persistence length and grafted density can ameliorate the irregular distribution of polymer beads in three-dimensional space as shown in Fig. 6. Therefore, a single chain in a crowded environment could maintain the rod-like shape and is not easy to entangle with other chains, and the number of kinks decreases correspondingly. Thus the thermal conductivity of a single chain increases accordingly as shown in Fig. 4b,

Figure 7 shows the overall thermal conductivity of different polymer brushes, and the thermal conductivities are typically anisotropic. $\kappa_{\perp}$ is predominantly influenced by the grafted density, as the weak van der Waals interactions between chains are the principal contributor to $\kappa_{\perp}$. Also, $\kappa_{\parallel}$ is significantly increased by increasing the grafted density, which is due to the alleviation of the bending of a polymer

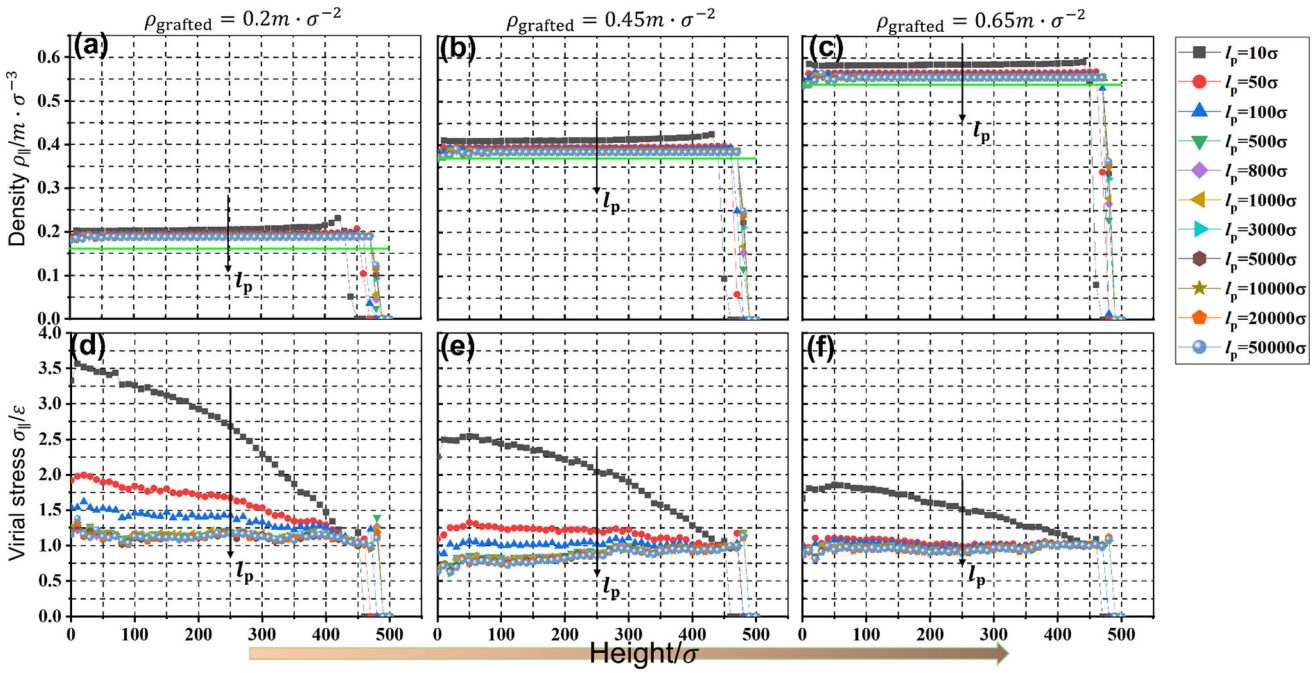

Figure 5 **a–c** The number density of different surface-initiated polymer brushes as a function of the height along the z direction. **d–f** The virial stress of different surface-initiated polymer brushes as a function of the height along the z direction. Data are shown for different grafted densities, and the black arrows indicate the increase in the persistence length.

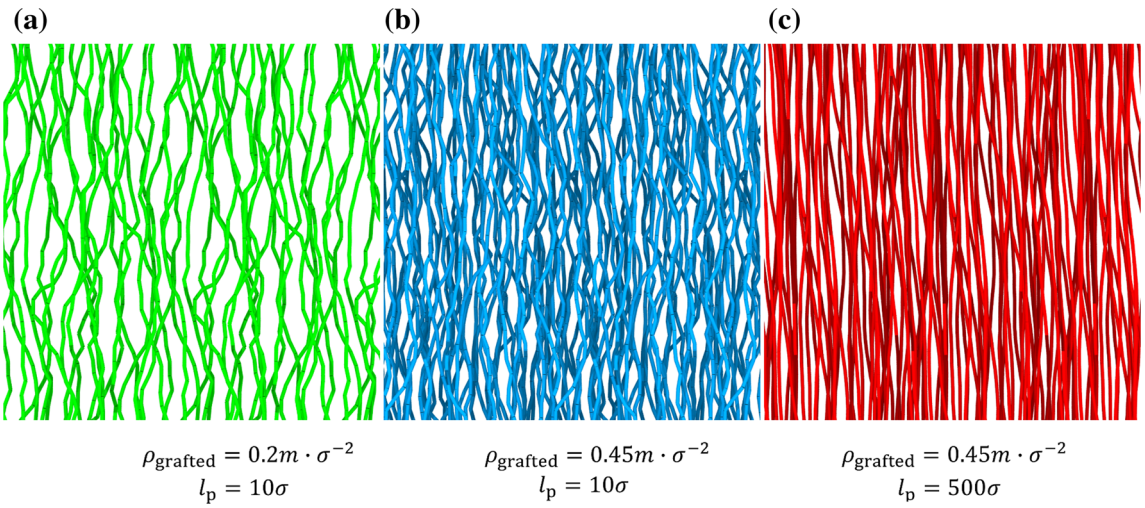

Figure 6 The morphology of different surface-initiated polymer brush systems captured from CGMD simulations.

chain in a crowded environment. To explain the influence of persistence length on thermal conductivity, we further make phonon analysis in the next part.

Phonon analysis

As phonons are the primary carrier of heat transfer in polymers, we analyze the phonon density of states (PDOS) to explain the change of $\kappa_{\|}$ in Fig. 8. The restraint in thermal conductivity of polymer brushes could be further attributed to the enhanced phonon scatterings, as evidenced by the phonon density of states. The PDOSs along the backbone direction are calculated separately for polymer brushes of different persistence lengths with the same grafted density of 0.65 $m \cdot \sigma^{-2}$. Besides, as the timestep is $\Delta t = 0.001\tau$, its inverse is almost the maximum attainable frequency.

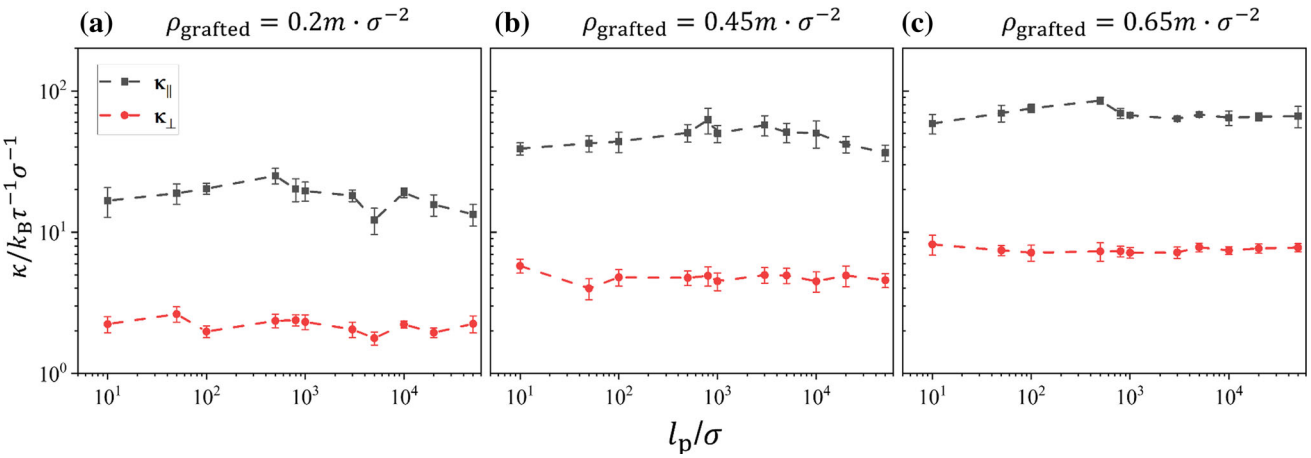

Figure 7 Thermal conductivity for surface-initiated polymer brushes with different grafted densities varying with the persistence length.

However, the PDOS curves decay to zero at about $50\tau^{-1}$. The results are shown in Fig. 8.

The PDOSs all concentrate on the low-frequency regime which is similar to the previous work [43], and it can be found that the high-frequency region of PDOSs is not sensitive to the change of the persistence length. Thus, we mainly focus on the change of the low-frequency region of PDOSs. As shown in Fig. 8a, with the increase in the persistence length, it can be seen that the peak of the low-frequency region is enhanced when $l_p < 800$, which means the increase in phonon group velocities and has a favorable effect on heat conduction. It also indicates that the increase of persistence length leads to the attenuation in phonon scattering and the increase in the thermal conductivity. However, when $l_p \geq 800$ the PDOS peaks in their low-frequency region are significantly damped, which induces the decrease in phonon group velocities and has an adverse effect on heat conduction. Although the overall PDOSs of polymer brushes with $l_p \geq 800$ show attenuation in low frequency, the peak of PDOSs with $l_p \geq 800$ is still higher than PDOSs with lower persistence length (e.g., $l_p = 10\sigma$) in the peak of the low-frequency region. Specially, as the persistence length keeps increasing, the curves of PDOS roughly overlap with each other, which indicates that they have almost the same phonon modes. Therefore, the thermal conductivity of polymer brushes with high persistence length is almost consistent shown in Fig. 7. The PDOS analysis may help explain the non-monotonic variation of longitudinal thermal conductivity $\kappa_{\parallel}$ shown in Fig. 7.

The PPRs of polymer brushes with the grafted density of $0.65\ m \cdot \sigma^{-2}$ varying with persistence length along the z direction are summarized in Fig. 9. From Fig. 9a, the increase in persistence length

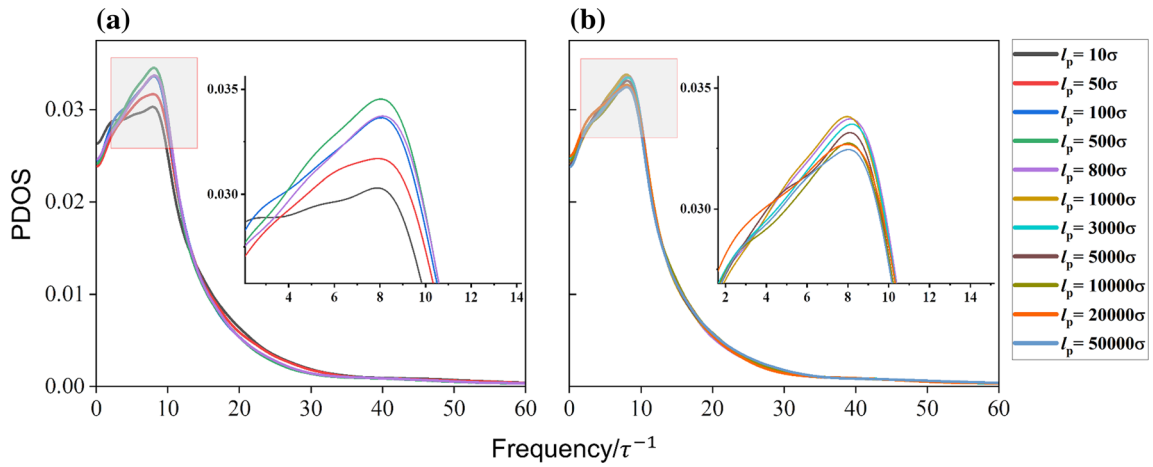

Figure 8 **a, b** PDOSs for surface-initiated polymer brushes with a grafted density of $0.65\ m \cdot \sigma^{-2}$ along the z direction.

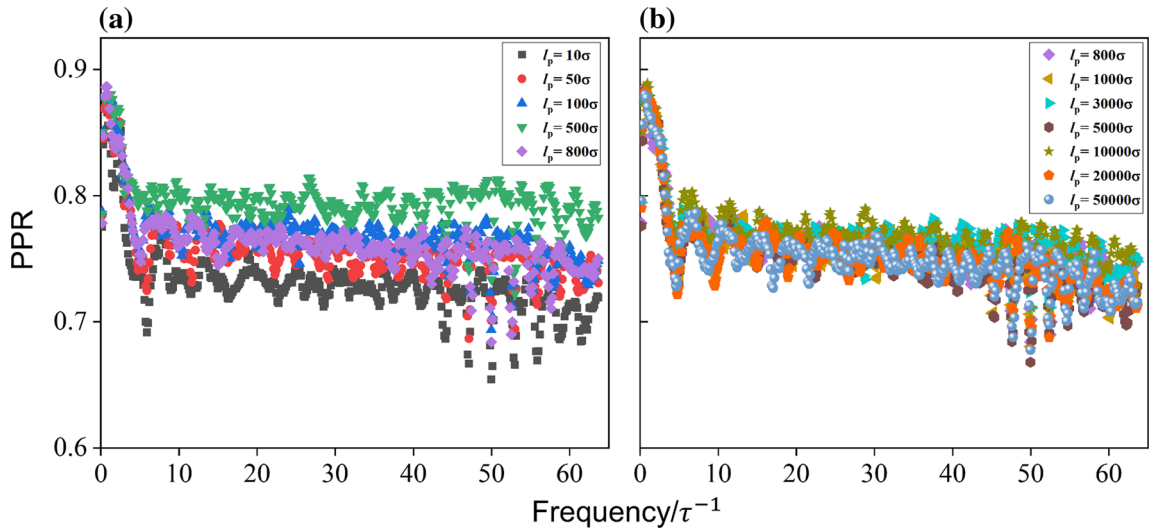

Figure 9 Phonon participation ratios for surface-initiated polymer brushes with the grafted density of 0.65 $m \cdot \sigma^{-2}$ along the z direction.

($l_p \leq 500\sigma$) leads to the increase in PPR over the entire range of frequency. Thus, phonon modes in polymer brushes tend to be delocalized, and more atoms participate in the motion. The delocalized phonons are capable of transporting thermal energy in polymer brushes, which results in an increment in thermal conductivity. As the persistence length of polymer brushes keeps increasing from Fig. 9b, the PPRs are almost close over the entire range of frequency which also proves the validity of PDOS analysis. However, the PPRs of polymer brushes with high persistence length are still higher than the PPRs of polymer brushes with low persistence length, e.g., the polymer brush with $l_p = 10\sigma$.

Conclusions

In summary, in-depth investigations of heat conduction in polymer brushes are performed using the CGMD simulations. A simple and useful mapping strategy is used to model one-dimensional and quasi-one-dimensional materials into CGMD models. We provide a feasible explanation for the attenuation of thermal conductivity in surface-initiated polymer brushes, i.e., the sharp reduction of $\kappa_{\|}$ in polymer brushes while a single polymer chain can have a high thermal conductivity. Although the reduction of thermal conductivity in polymer brushes is inevitable, we find that the $\kappa_{\|}$ can be significantly improved by tuning the grafted density and the persistence length of polymer chains, and the mechanism is explained using the structure and phonon analysis. We demonstrate that the polymer brushes consisting of one-dimensional materials or quasi-one-dimensional materials are found to have controllable thermal conductivity, thus indicating their potential applications in heat dissipation coatings. We also show a numerical verification that a reasonable selection and design of structure can effectively broaden the application of existing materials. Therefore, upon experimental validation, these results may help design advanced coating materials with controllable thermal properties.

Acknowledgements

The computations in this work were run on the π 2.0 cluster supported by the Center for High Performance Computing at Shanghai Jiao Tong University.

Funding

The author(s) disclosed receipt of the following financial support for the research, authorship, and/or publication of this article: this work was supported by the National Natural Science Foundation of China (Grant No. 11972226).

Data availability

The input files for LAMMPS simulations are available from the corresponding author upon reasonable request.

Declarations

Conflict of interest The authors declared no potential conflicts of interest with respect to the research, authorship, and/or publication of this article.

References

[1] Guo ZB, Sha WH, Yao HM (2019) Measuring thermal conductivity of ultra-small materials exampled by the reaction chambers of bombardier beetles. Int J Heat Mass Transf 134:1318–1322. https://doi.org/10.1016/j.ijheatmasstransfer.2019.02.059

[2] Lee V, Wu CH, Lou ZX, Lee WL, Chang CW (2017) Divergent and ultrahigh thermal conductivity in millimeter-long nanotubes. Phys Rev Lett 118:135901. https://doi.org/10.1103/PhysRevLett.118.135901

[3] Nadjahi C, Louahlia H, Lemasson S (2018) A review of thermal management and innovative cooling strategies for data center. Sust Comput 19:14–28. https://doi.org/10.1016/j.suscom.2018.05.002

[4] Bao H, Chen J, Gu X, Cao B (2018) A review of simulation methods in micro/nanoscale heat conduction. ES Energy Environ 1:16–55. https://doi.org/10.30919/esee8c149

[5] Giussi JM, Cortez ML, Marmisolle WA, Azzaroni O (2019) Practical use of polymer brushes in sustainable energy applications: interfacial nanoarchitectonics for high-efficiency devices. Chem Soc Rev 48:814–849. https://doi.org/10.1039/C8CS00705E

[6] Mukherji D, Singh MK (2021) Tuning thermal transport in highly cross-linked polymers by bond-induced void engineering. Phys Rev Mater 5:025602. https://doi.org/10.1103/PhysRevMaterials.5.025602

[7] Choy CL, Wong YW, Yang GW, Kanamoto T (1999) Elastic modulus and thermal conductivity of ultradrawn polyethylene. J Polym Sci B Polym Phys 37:3359–3367. https://doi.org/10.1002/(SICI)1099-0488(19991201)37:23%3c3359::AID-POLB11%3e3.0.CO;2-S

[8] Shen S, Henry A, Tong J, Zheng R, Chen G (2010) Polyethylene nanofibres with very high thermal conductivities. Nat Nanotech 5:251–255. https://doi.org/10.1038/nnano.2010.27

[9] Henry A (2014) Thermal transport in polymers. Annu rev heat transf 17:485–520. https://doi.org/10.1615/AnnualRevHeatTransfer.2013006949

[10] Ruscher C, Rottler J, Boott CE, MacLachlan MJ, Mukherji D (2019) Elasticity and thermal transport of commodity plastics. Phys Rev Mater 3:125604. https://doi.org/10.1103/PhysRevMaterials.3.125604

[11] Jakubinek MB, White MA, Li G, Jayasinghe C, Cho WD, Schulz MJ, Shanov V (2010) Thermal and electrical conductivity of tall, vertically aligned carbon nanotube arrays. Carbon 48:3947–3952. https://doi.org/10.1016/j.carbon.2010.06.063

[12] Kumanek B, Janas D (2019) Thermal conductivity of carbon nanotube networks: a review. J Mater Sci 54:7397–7427. https://doi.org/10.1007/s10853-019-03368-0

[13] Yamaguchi S, Tsunekawa I, Komatsu N, Gao WL, Shiga T, Kodama T, Kono J, Shiomi J (2019) One-directional thermal transport in densely aligned single-wall carbon nanotube films. Appl Phys Lett 115:223104. https://doi.org/10.1063/1.5127209

[14] Feser JP, Sadhu JS, Azeredo BP, et al (2012) Thermal conductivity of silicon nanowire arrays with controlled roughness. J Appl Phys 112:114306. https://doi.org/10.1063/1.4767456

[15] Henry A, Chen G, Plimpton SJ, Thompson A (2010) 1D-to-3D transition of phonon heat conduction in polyethylene using molecular dynamics simulations. Phys Rev B 82:144308–5. https://doi.org/10.1103/PhysRevB.82.144308

[16] Crnjar A, Melis C, Colombo L (2018) Assessing the anomalous superdiffusive heat transport in a single one-dimensional PEDOT chain. Phys Rev Mater 2:015603. https://doi.org/10.1103/PhysRevMaterials.2.015603

[17] Feng C, Huang XY (2018) Polymer brushes: efficient synthesis and applications. Acc chem res 51:2314–2323. https://doi.org/10.1021/acs.accounts.8b00307

[18] Ritsema GC, Veldscholte LB, Nijkamp J, Beer S (2020) Sorption characteristics of polymer brushes in equilibrium with solvent vapors. Macromolecules 53:8428–8437

[19] Roy A, Bougher TL, Geng R, Ke YT, Locklin J, Cola BA (2016) Thermal conductance of poly(3-methylthiophene) brushes. ACS Appl Mater Interface 8:25578–25585. https://doi.org/10.1021/acsami.6b04429

[20] Bhardwaj A, Phani AS, Nojeh A, Mukherji D (2021) Thermal transport in molecular forests. ACS Nano 15:1826–1832. https://doi.org/10.1021/acsnano.0c09741

[21] van den Akker CC, Engel M, Velikov KP, Bonn M, Koenderink G (2011) Morphology and persistence length of amyloid fibrils are correlated to peptide molecular structure. J Am Chem Soc 133:18030–18033. https://doi.org/10.1021/ja206513r

[22] Hoogendam CW, Keizer A, Stuart MA, et al (1998) Persistence length of carboxymethyl cellulose as evaluated from size exclusion chromatography and potentiometric titrations. Macromolecules 31:6297–6309. https://doi.org/10.1021/ma971032i

[23] Ramachandran R, Beaucage G, Kulkarni AS, McFaddin D, Merrick-Mack J, Galiatsatos V (2008) Persistence length of short-chain branched polyethylene. Macromolecules 41:9802–9806. https://doi.org/10.1021/ma801775n

[24] Fakhri N, Tsyboulski DA, Cognet L, Weisman RB, Pasquali M (2009) Diameter-dependent bending dynamics of single-walled carbon nanotubes in liquids. Proc Nal Acad Sci 106:14219–14223. https://doi.org/10.1073/pnas.0904148106

[25] Dunbar M, DeBenedictis E, Keten S (2019) Dimerization energetics of curli fiber subunits CsgA and CsgB. Npj Comput Mater 5:27–36. https://doi.org/10.1038/s41524-019-0164-5

[26] Manning GS (2006) The persistence length of DNA is reached from the persistence length of its null isomer through an internal electrostatic stretching force. Biophys J 91:3607–3616. https://doi.org/10.1529/biophysj.106.089029

[27] Wignall GD, Schelten J, Ballard DGH (1974) Measurements of radius of gyration and persistence length in bulk atactic polystyrene by low-angle neutron scattering. J Appl Crystallogr 7:190–190. https://doi.org/10.1107/S0021889874009204

[28] Liu H, Song HL, Feng XQ, Yang JL (2014) Surface effects on the persistence length of nanowires and nanotubes. Theor Appl Mech Lett 4:051009. https://doi.org/10.1063/2.1405109

[29] Brandrup JI, Immergut EH, Grulke EA (2003) Polymer handbook, 4th edn. Hoboken, Wiley-Interscience

[30] Sha WH, Fu JM, Guo FL (2021) Wetting characteristics of polymer adhesives with different chain bending stiffness. High Perform Polym 33:1220–1229. https://doi.org/10.1177/09540083211035016

[31] Kremer K (1990) Dynamics of entangled linear polymer melts: a molecular-dynamics simulation. J Chem Phys 92:5057–5086. https://doi.org/10.1063/1.458541

[32] Plimpton S (1995) Fast parallel algorithms for short-range molecular dynamics. J Comput Phys 117:1–19. https://doi.org/10.1006/jcph.1995.1039

[33] Yaghoobi P, Moghaddam MV, Nojeh A (2011) "Heat trap": light-induced localized heating and thermionic electron emission from carbon nanotube arrays. Solid State Commun 151:1105–1108. https://doi.org/10.1016/j.ssc.2011.05.024

[34] Fan ZY, Pereira LF, Wang HQ, Zheng JC, Donadio D, Harju A (2015) Force and heat current formulas for many-body potentials in molecular dynamics simulations with applications to thermal conductivity calculations. Phys Rev B 92:094301. https://doi.org/10.1103/PhysRevB.92.094301

[35] Boone P, Babaei H, Wilmer CE (2019) Heat flux for many-body interactions: corrections to LAMMPS. J Chem Theory Comput 15:5579–5587. https://doi.org/10.1021/acs.jctc.9b00252

[36] Manav M, Ponga M, Phani AS (2019) Stress in a polymer brush. J Mech Phys Sol 127:125–150. https://doi.org/10.1016/j.jmps.2019.03.009

[37] Dickey JM, Paskin A (1969) Computer simulation of the lattice dynamics of solids. Phys Rev 188:1407–1418. https://doi.org/10.1103/PhysRev.188.1407

[38] Liang T, Zhang P, Yuan P, Zhai SP (2018) In-plane thermal transport in black phosphorene/graphene layered heterostructures: a molecular dynamics study. Phys Chem Chem Phys 20:21151–21162. https://doi.org/10.1039/C8CP02831A

[39] Liang T, Zhou M, Zhang P, Yuan P, Yang DG (2020) Multilayer in-plane graphene/hexagonal boron nitride heterostructures: insights into the interfacial thermal transport properties. Int J Heat and Mass Transfer 151:119395. https://doi.org/10.1016/j.ijheatmasstransfer.2020.119395

[40] Loh GC, Teo E, Tay BK (2012) Phonon localization around vacancies in graphene nanoribbons. Diam Relat Mater 23:88–92. https://doi.org/10.1016/j.diamond.2012.01.006

[41] Henry A, Chen G (2008) High thermal conductivity of single polyethylene chains using molecular dynamics simulations. Phys Rev Lett 101:235502. https://doi.org/10.1103/PhysRevLett.101.235502

[42] Zhang Z, Chen J (2018) Thermal conductivity of nanowires. Chin Phys B 27:035101. https://doi.org/10.1088/1674-1056/27/3/035101

[43] Huo R, Zhang Z, Athir N, Fan YH, Liu J, Shi L (2020) Designing high thermal conductivity of cross-linked epoxy resin via molecular dynamics simulations. Phys Chem Chem Phys 22:19735–19745. https://doi.org/10.1039/D0CP02819C